https://doi.org/10.5194/egusphere-2026-6186
Preprint. Discussion started: 20 November 2026
© Author(s) 2026. CC BY 4.0 License.

# Evaluating lake surface water temperature as an indicator of ice phenology in Selin Co, Tibetan Plateau

Beibei He[1,2], Donghui Shangguan[1,2,3], Da Li[1,4], Jinkui Wu[1,2], Rongjun Wang[1,4], and Yaojun Li[1,2]

[1]Tanggula Mountain Cryosphere and Environment Observation and Research Station of Tibet Autonomous Region, State Key Laboratory of Cryospheric Science and Frozen Soil Engineering, Northwest Institute of Eco-Environment and Resources, Chinese Academy of Sciences, Lanzhou 730000, China

[2]University of Chinese Academy of Sciences, Beijing 100049, China

[3]China–Pakistan Joint Research Center on Earth Sciences, CAS-HEC, Islamabad 45320, Pakistan

[4]Midui Glacier-Guangxie Lake Disaster Field Science Observation and Research Station of Tibet Autonomous Region, Nyingchi 860000, China

Correspondence: Donghui Shangguan (dhguan@lzb.ac.cn)

**Abstract.** Satellite-derived lake surface water temperature (LSWT) is increasingly used to determine lake ice phenology, commonly assuming that freezing and melting occur when LSWT crosses 0°C. Here, we tested this assumption in Selin Co, a large saline lake on the central Tibetan Plateau, using MODIS LSWT (2001–2025), ERA5-Land meteorological data, optical ice phenology observations spanning 20 ice seasons, and in situ water-temperature and conductivity profiles. Within the perennial lake area, nighttime LSWT increased by 0.55°C per decade, while daytime LSWT showed no significant trend, resulting in a 0.39°C per decade decline in diurnal range. Freezing began 3–5 weeks after air temperature fell below 0°C, when whole-lake mean LSWT remained near 4°C, and complete freeze-up followed ~46 days later. Because the lake's practical salinity of 8 lowers the temperature of maximum density to 2.2°C, the water column continued convective cooling below 4°C before freeze-up. Thus, complete freeze-up was governed primarily by lake-water cooling rather than the onset of atmospheric cooling, whereas ice melt began weeks before air temperature became positive and was associated with winter warming and solar radiation. A 0°C LSWT threshold produced 2–5-week biases for three of four ice events and reproduced only complete freeze-up well after threshold correction. These results highlight the roles of lake depth, salinity, and heat storage in satellite-based lake ice phenology retrievals for large saline lakes.

## 1 Introduction

Although lakes occupy less than 3% of the global land surface, they store approximately 87% of the world's surface liquid freshwater and constitute an important component of the hydrological and energy cycles (Yao et al., 2023). By altering surface radiation balance, sensible heat flux, latent heat flux, and atmospheric moisture supply, lakes exert significant influences on local and regional climates (Zhu et al., 2025; Qiu et al., 2025). The Tibetan

https://doi.org/10.5194/egusphere-2026-6186
Preprint. Discussion started: 20 November 2026
© Author(s) 2026. CC BY 4.0 License.

Plateau and its surrounding mountains, often referred to as the "Third Pole" and the "Asian Water Tower," contain the largest stores of snow, glacier, and lake water resources outside the polar regions (Yao et al., 2022). The plateau hosts more than 50,000 km² of lakes, including approximately 1,400 lakes larger than 1 km² (Zhang et al., 2022). Under the combined influence of strong solar radiation, a cold and dry atmospheric environment, and large diurnal temperature variations, lake heat storage and energy exchange processes are highly sensitive to climate change. Abrupt changes in surface albedo during lake ice formation and melt can further amplify temperature anomalies (Shi et al., 2025). Since the 1950s, the Tibetan Plateau has warmed at a rate of approximately 0.16–0.67°C per decade (Kuang and Jiao, 2016). The combined effects of climate warming and wetting, together with cryospheric degradation, have reshaped the thermal regimes of lakes across the plateau (Kirillin et al., 2017; Bibi et al., 2018; Guo et al., 2022).

Lake surface water temperature (LSWT) is a key indicator of the thermal state of lakes and their energy exchange with the atmosphere, while also providing the thermal background for lake ice formation and melt (Woolway et al., 2020). As natural heat reservoirs, lakes influence regional climate through radiative heat absorption and evaporative cooling (Rouse et al., 2003; Piccolroaz et al., 2024). Warmer lakes release more energy through evaporation and longwave radiation (Schmid et al., 2014). Global analyses indicate that, under equilibrium conditions, lake surface waters warm by approximately 70%–85% as much as air temperature, with lake warming generally lagging behind atmospheric warming because of enhanced evaporative cooling (Schmid et al., 2014; Tong et al., 2023). Most lakes on the Tibetan Plateau have experienced warming in recent decades (Wan et al., 2018), with warming rates of 0.01–0.47°C per decade during 1978–2017 and substantially stronger warming in winter than in summer (Guo et al., 2022). Delayed freeze-up and earlier ice melt shorten the ice-covered season (Li et al., 2022), reducing surface albedo and potentially increasing the frequency of lake heatwaves (Zhang and Yao, 2023; Woolway et al., 2021; Wang et al., 2024).

Thermal infrared remote sensing enables continuous observations of lake surface temperature during both day and night and provides approximately twice as many cloud-free observation opportunities as optical lake ice mapping, making LSWT time series widely used for extracting lake ice phenology (Nonaka et al., 2007; Zhang et al., 2021; Hou et al., 2022). Most studies identify the first day on which LSWT remains below or above 0°C for several consecutive days as the onset of freeze-up or ice melt, respectively (e.g., Shi et al., 2024). Other studies calibrate lake-specific thresholds using optical lake ice products (Wu et al., 2022). The 0°C criterion implicitly assumes that the whole-lake mean surface temperature has fallen to the

https://doi.org/10.5194/egusphere-2026-6186
Preprint. Discussion started: 20 November 2026
© Author(s) 2026. CC BY 4.0 License.

freezing point when lake ice forms. However, in large and deep lakes, ice initially forms in shallow and sheltered areas, while open-water regions may still retain substantial heat accumulated during summer. Consequently, changes in whole-lake mean LSWT and ice-cover conditions are not necessarily synchronous. Moreover, the temperature of an ice-covered surface can fall well below 0°C, meaning that satellite-derived LSWT during the ice-covered period may represent ice or snow surface temperature rather than water temperature (Kirillin et al., 2012). Dissolved salts further complicate this process. Salinity not only lowers the freezing point of lake water but also substantially alters the temperature of maximum density. For freshwater, the temperature of maximum density is approximately 4°C, and this parameter determines the cessation of autumnal convection and the formation of the cold surface layer (Boehrer and Schultze, 2008). Most lakes on the Tibetan Plateau are brackish or saline, yet such salinity-related thermal effects have rarely been considered when using LSWT to identify lake ice events.

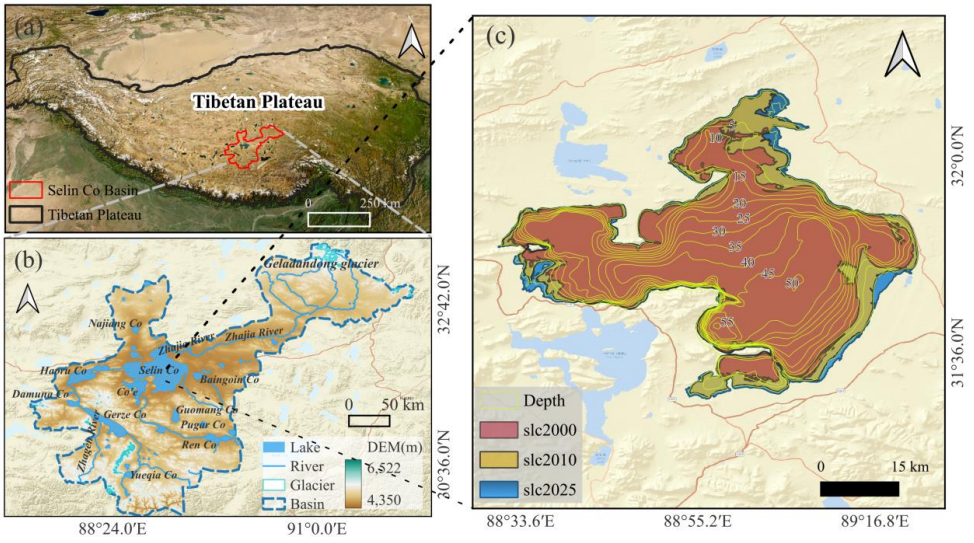
The links between air temperature, LSWT and ice have mostly been examined pairwise and at regional scale. Air temperature is the usual predictor of ice timing (Kropáček et al., 2013; Cai et al., 2019), and LSWT is known to lag air temperature because of heat storage (Schmid et al., 2014; Kirillin et al., 2017). For individual large lakes, however, the extent to which atmospheric cooling is translated into lake freezing through changes in lake thermal state, the timescale of this transition, and whether the same coupling operates during ice melt remain poorly quantified (Brown and Duguay, 2010; Murfitt and Brown, 2017). Rapid lake expansion (Xu et al., 2024) also introduces challenges for satellite remote sensing. Fixed-date lake masks can mix newly inundated littoral zones with open water, thereby affecting the accuracy of LSWT retrievals.

Selin Co is a large saline lake on the Tibetan Plateau that has undergone rapid expansion in recent decades and has an independent optical lake ice phenology record (Chen et al., 2021; Li et al., 2023), making it an ideal site for such validation. We combined MODIS LSWT, ERA5-Land meteorological data, the above lake ice phenology record, and in situ profiles of water temperature and electrical conductivity to address four questions. After accounting for lake expansion, how does LSWT vary across interannual and monthly timescales and among different stages of the ice season? How are air temperature, LSWT, and lake ice coupled throughout the freeze-thaw cycle? How do lake heat storage and salinity regulate this coupling? To what extent can LSWT thresholds, including the commonly used 0°C criterion, reproduce the timing and interannual variability of lake ice events in Selin Co?

https://doi.org/10.5194/egusphere-2026-6186
Preprint. Discussion started: 20 November 2026
© Author(s) 2026. CC BY 4.0 License.

## 2 Study area

Selin Co (31.6–32.1° N, 88.5–89.4° E) is located in the southern Qiangtang Plateau in the central Tibetan Plateau, at the junction of Shenzha, Banga, and Nyima counties (Fig. 1a). It is the largest lake in the Tibet Autonomous Region and has an elongated east–west orientation. The lake basin was historically a closed inland drainage basin. In September 2023, the lake began to overflow and discharge into the neighboring Bangong Co (Lei et al., 2024). The lake is saline, with a reported salinity of 7.8 g $L^{-1}$ and a pH range of 9.2–9.8 (Zhu and Wang, 2021). In situ conductivity measurements collected in 2017 correspond to a practical salinity of approximately 8. The Selin Co basin covers an area of approximately 45,530 km² and is mainly fed by the Zhagacangbu and Zhagencangbu Rivers (Fig. 1b). The maximum lake depth has been reported to be approximately 59 m (Gyawali et al., 2019). The study area is located in a climatic transition zone between the Indian monsoon and the mid-latitude westerlies and is characterized by a cold and arid climate. The mean annual air temperature is −1.8°C, with an annual precipitation of 389.4 mm. Air temperatures remain above 0 °C from May to September, which also coincides with the peak precipitation period. Winter snowfall is mainly supplied by the mid-latitude westerlies. The lake area grew from 1,617 km² in the 1970s to about 2,455 km² in 2025 (Fig. 1c), a rapid expansion attributed to increased precipitation, which averaged 398 mm per year over 1990–2020, and to accelerated glacier melt, evidenced by the sustained shrinkage of glaciers in the basin over the past 30 years (Zhou et al., 2015; Chen et al., 2021). Since 2000, regional warming has intensified, further altering hydrological processes across the basin (Zhou et al., 2015).



https://doi.org/10.5194/egusphere-2026-6186
Preprint. Discussion started: 20 November 2026
© Author(s) 2026. CC BY 4.0 License.

**Figure 1.** Overview of the study area. (a) Location of the Selin Co basin on the Tibetan Plateau. (b) Topography of the basin with the major rivers, glaciers and lakes. (c) Bathymetry of Selin Co from digitized depth surveys (Gyawali et al., 2019) and lake boundaries in 2000, 2010 and 2025.

## 3 Data and methods

### 3.1 Data

#### 3.1.1 MODIS land surface temperature

Daytime and nighttime LSWT were obtained from the MODIS Terra land surface temperature products MOD11A1 (daily) and MOD11A2 (8-day composite), Collection 6.1, at a spatial resolution of 1 km (Wan, 2014). The standard satellite overpass times are approximately 10:30 and 22:30 local solar time, respectively. The daily product was used to analyze lake-atmosphere coupling and lake ice phenology, whereas the 8-day composite product was used for trend analysis. Seasonal mean LSWT and Sen's slope were calculated on a pixel-by-pixel basis for 2001–2025.

#### 3.1.2 Lake-ice phenology

Lake ice phenology data for the 2000/01–2020/21 ice seasons were obtained from the dataset developed by Li et al. (2023). The dataset provides daily lake ice maps derived from 250 m MODIS Terra surface reflectance data, with lake boundaries extracted from Landsat imagery. The dataset achieved an overall accuracy of 94% during the freeze-up period, with a Kappa coefficient above 0.89. Four key phenological events were identified for each ice season, including freeze-up start (FUS), freeze-up end (FUE), defined as complete freeze-up, break-up start (BUS), and break-up end (BUE). We selected the 20 ice seasons overlapping with the LSWT record, spanning 2001/02 to 2020/21.

#### 3.1.3 ERA5-Land meteorology

Daily mean, maximum and minimum 2 m air temperature, downward shortwave radiation, snowfall and 10 m wind speed for 2000–2025 were taken from the ERA5-Land reanalysis (Muñoz-Sabater et al., 2021) through Google Earth Engine. Daily wind speed was calculated as the mean of hourly wind speeds derived from the u and v wind components. For each variable, we calculated the spatial mean of ERA5-Land grid cells located within 30 m inside the lake shoreline delineated in 2001. Because air temperature over lake grid cells in ERA5-Land may be partly influenced by the lake parameterization scheme used in the reanalysis, we additionally extracted the same variables from a terrestrial annulus extending 10–30 km beyond the lake shoreline to assess whether the results were sensitive to the source of air temperature

https://doi.org/10.5194/egusphere-2026-6186
Preprint. Discussion started: 20 November 2026
© Author(s) 2026. CC BY 4.0 License.

data.

### 3.1.4 In situ water temperature and conductivity

Water temperature and electrical conductivity recorded hourly by HOBO conductivity loggers moored at 2, 15, 18, 28 and 38 m depth in the southern part of the lake (31°45′26″ N, 88°58′22″ E) from 22 June to 13 December 2017 were obtained from the National Tibetan Plateau Environment Data Center (Wang, 2019). The observations covered summer thermal stratification, autumn cooling, and the first three weeks after the onset of lake freezing. Measurements recorded when the instruments were out of water and on the first day of deployment were excluded, and the remaining hourly observations were averaged to daily values. For the remaining 172 days, MODIS LSWT showed a correlation coefficient of 0.96 with the daily mean water temperature at 2 m depth, with a mean bias of −0.6°C and a root mean square deviation of 1.2°C (Fig. 2).

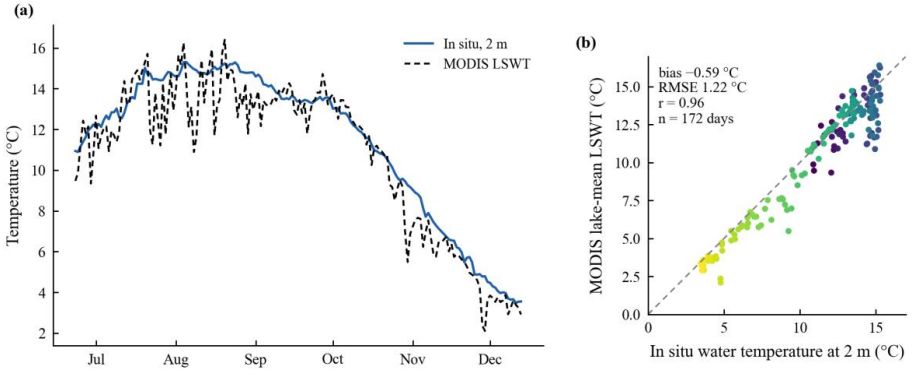



**Figure 2.** Comparison of daily MODIS LSWT with water temperature measured at 2 m depth in Selin Co, June–December 2017 (Wang, 2019). (a) Time series. (b) MODIS lake-mean LSWT against the in-situ temperature.

## 3.2 Methods

### 3.2.1 Lake extents and LSWT series

Lake extents for 2001 and 2010 were taken from the boundaries of the Li et al. (2023) dataset, which were delineated from Landsat imagery. Extents from 2023 onward were mapped from cloud-free Landsat 8 OLI surface reflectance images acquired during the ice-free season with the modified normalized difference water index (MNDWI) (Xu, 2006):

$$MNDWI = \frac{\rho_{Green} - \rho_{SWIR}}{\rho_{Green} + \rho_{SWIR}}$$

where $\rho_{Green}$ and $\rho_{SWIR}$ are the reflectances in the green and shortwave infrared bands. The masks were checked against shoreline morphology and manual inspection to remove

https://doi.org/10.5194/egusphere-2026-6186
Preprint. Discussion started: 20 November 2026
© Author(s) 2026. CC BY 4.0 License.

misclassification from cloud shadow, snow, ice and mixed shoreline pixels, and they were eroded inward by one to two pixels to reduce thermal contamination from the shore. LSWT was summarized within the 2001 extent, which approximates the permanent water body, and within the 2025 extent, which includes the newly inundated margins.

Gaps in the daily MOD11A1 series caused by cloud and retrieval failure were filled in two stages, with seasonal decomposition recovering the regular annual cycle and linear interpolation bridging short gaps, and the series was smoothed with a 7 d moving average. Annual means were built from monthly means of the 8 d composites, and years with missing months were excluded. Four ice phases were defined in each season from the phenology record, open water from BUE to the following FUS, freeze-up from FUS to FUE, complete ice cover from FUE to BUS and break-up from BUS to BUE.

#### 3.2.2 Coupling between LSWT and air temperature

Climatological annual cycles of LSWT and air temperature were used to characterize seasonal hysteresis. Cross-correlations were calculated for 7-day-smoothed raw and anomaly series, with anomalies referenced to the 31-day smoothed daily climatology. Anomaly correlations were further calculated separately for September–January and February–June. Negative lags indicate that LSWT changes lag behind air temperature. For each ice phenology stage, interannual relationships between stage-mean LSWT and air temperature were assessed using correlation and linear regression based on the 2001 lake extent. Daytime LSWT was paired with daily maximum air temperature, and nighttime LSWT with daily minimum air temperature.

#### 3.2.3 Freeze–thaw cascade and LSWT thresholds

were identified as the first day of at least five consecutive days below the threshold from 1 September to 31 March, or above the threshold from 1 February to 31 July. The freeze-up sequence included sustained sub-zero air temperature, LSWT reaching 4°C, FUS, LSWT reaching 0°C, and FUE. The break-up sequence included LSWT reaching 0°C, BUS, sustained above-zero air temperature, and BUE. Lag times between consecutive events and interannual correlations between ice events and threshold-crossing dates were calculated. LSWT and air temperature on each event date were extracted, freezing and thawing degree-days were accumulated from 1 October and 1 February, respectively, and 60-day composites of the temperature difference ($\Delta T$) before and after each event were constructed.

To assess LSWT thresholds for ice phenology detection, event dates were identified using thresholds from −6 to 8 °C at 0.25 °C intervals with the same persistence criterion. For each

https://doi.org/10.5194/egusphere-2026-6186
Preprint. Discussion started: 20 November 2026
© Author(s) 2026. CC BY 4.0 License.

event and threshold, mean bias, RMSE, and interannual correlation with observed ice phenology were calculated. The optimal threshold minimized RMSE and was selected using leave-one-ice-season-out cross-validation. Trends in LSWT-derived event dates were then compared with those from observed ice phenology.

## 4 Results

### 4.1 Long-term change and spatial pattern of LSWT

From 2001 to 2025, nighttime LSWT within the 2001 perennial lake extent increased steadily at approximately 0.55°C per decade, whereas daytime LSWT showed substantial interannual variability but no significant trend (Fig. 3a; Table 1), resulting in a declining diurnal temperature range (Fig. 3b). In the surrounding terrestrial annulus, daily maximum and minimum air temperatures increased by approximately 0.60 and 0.45°C per decade, respectively, with no significant trend in air temperature range (Fig. 3c). The asymmetric LSWT trends therefore originated from the lake surface itself. Nighttime LSWT warmed slightly faster than nighttime air temperature, whereas daytime LSWT warming was less than one-fifth of daytime air temperature warming. Daytime heat is mixed into deeper waters, weakening the lake surface response to atmospheric warming (Toffolon et al., 2014), while enhanced evaporation under daytime warming may further suppress this response (Tong et al., 2023). At night, stored heat is released gradually, sustaining surface temperatures. Thus, the asymmetry reflects different lake–atmosphere coupling between day and night rather than changes in the atmospheric diurnal cycle. Trend signs were consistent across most subperiods lasting at least 10 years (Fig. 3d, e). Nighttime warming emerged only in longer periods including recent years, whereas declining DTD was detectable across more periods, including 2001–2020.

**Table 1.** Trends in annual mean LSWT and DTD within the 2001 and 2025 lake extents (°C per decade), with 95% confidence intervals and Mann–Kendall p values corrected for serial correlation.

| Series | Slope 2001–2025 | 95% CI | p | Slope 2001–2020 | p |
|---|---|---|---|---|---|
| Daytime LSWT, 2001 extent | +0.11 | −0.15 to +0.32 | 0.315 | −0.06 | 0.922 |
| Daytime LSWT, 2025 extent | −0.26 | −0.55 to +0.01 | 0.053 | −0.48 | 0.012 |
| Nighttime LSWT, 2001 extent | +0.55 | +0.20 to +0.85 | 0.007 | +0.36 | 0.163 |
| Nighttime LSWT, 2025 extent | +0.91 | +0.54 to +1.26 | <0.001 | +0.85 | 0.005 |
| DTD, 2001 extent | −0.39 | −0.55 to −0.21 | <0.001 | −0.32 | 0.018 |
| DTD, 2025 extent | −0.91 | −1.38 to −0.67 | <0.001 | −0.93 | <0.001 |

https://doi.org/10.5194/egusphere-2026-6186
Preprint. Discussion started: 20 November 2026
© Author(s) 2026. CC BY 4.0 License.

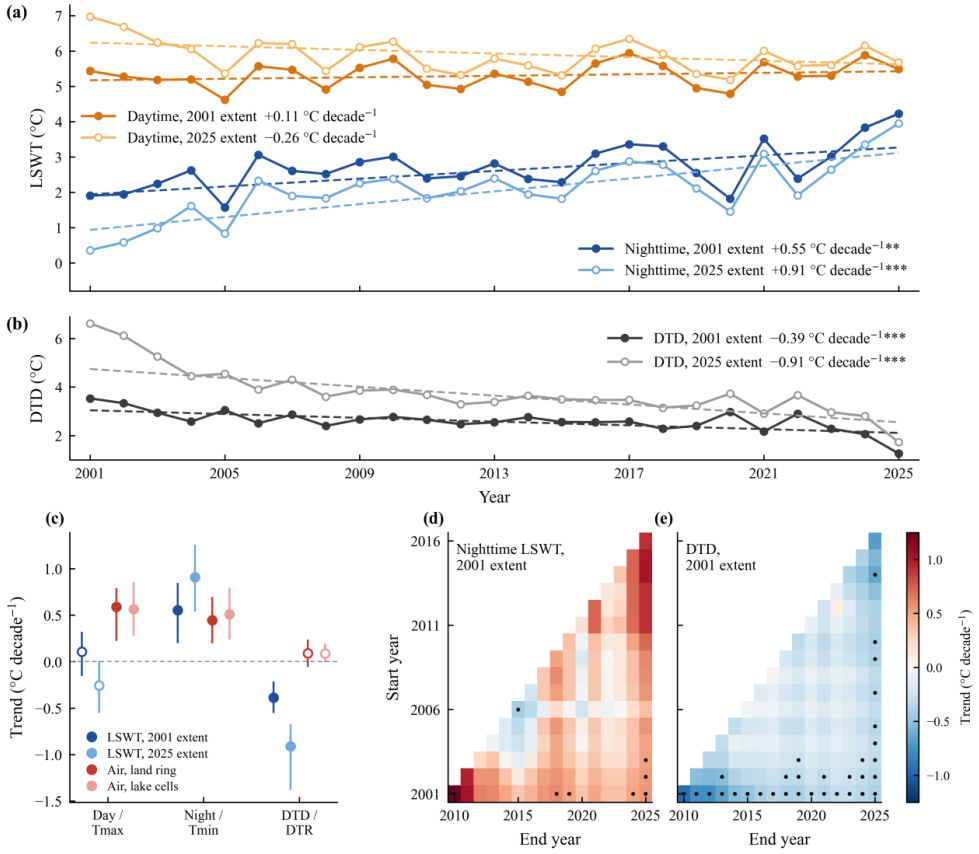



**Figure 3.** Interannual variation of LSWT over Selin Co, 2001–2025. (a) Annual mean daytime and nighttime LSWT within the 2001 and 2025 lake extents with their Sen's slopes. (b) Diurnal temperature difference (DTD). (c) Trends of LSWT compared with those of ERA5-Land air temperature over a land ring around the lake and over the lake cells. (d, e) Trends of nighttime LSWT and DTD within the 2001 extent for all periods of at least 10 years. Dots mark trends with $p < 0.05$.

Seasonal maps show that the whole-lake mean trends represent the broader open-water area (Fig. 4). Across open water, daytime LSWT trends were near zero in all seasons, whereas nighttime trends were consistently positive. Trend fields were spatially coherent, except in winter when lake ice produced more fragmented patterns. Anomalous areas were confined to narrow shoreline belts. These areas were warmer by day and cooler at night than the lake interior because shallow water and mixed land–water pixels respond more strongly to the diurnal cycle. In expanding shoreline areas, significant daytime cooling and nighttime warming reflected land inundation (Guo et al., 2025), which explains the stronger trends within the 2025 lake extent than within the perennial extent (Table 1).

https://doi.org/10.5194/egusphere-2026-6186
Preprint. Discussion started: 20 November 2026
© Author(s) 2026. CC BY 4.0 License.

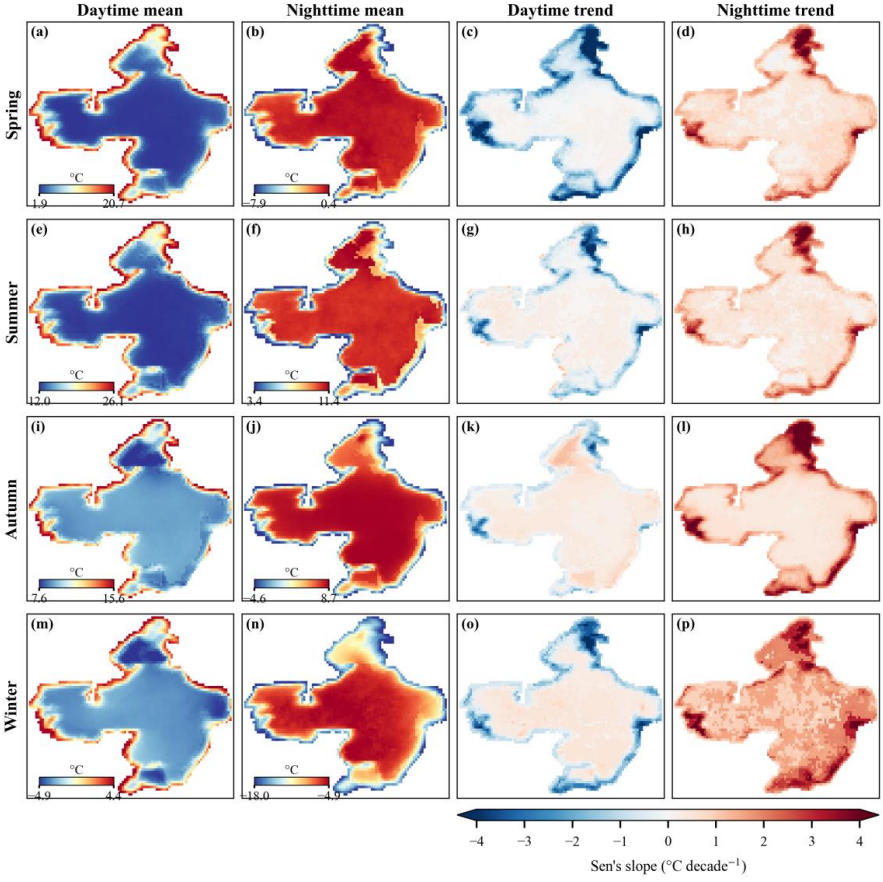



**Figure 4.** Seasonal mean daytime and nighttime LSWT (a-n) and their trends (e-p) over Selin Co for spring, summer, autumn and winter, 2001–2025.

### 4.2 Seasonal and ice-regime structure of LSWT trends

Warming in the permanent lake area was concentrated during the cooling half of the year (Fig. 5a). Nighttime LSWT increased most clearly from September to December, and daytime LSWT warmed only in November and December. The margins of the 2025 extent added daytime cooling mainly in spring, when bare shorelands heat rapidly under strong radiation while the lake is still frozen or close to 0 °C.

When LSWT was averaged over the lake's own ice phases instead of calendar months, none of the phase-mean trends of the permanent water body reached $p < 0.05$ (Fig. 5b). The early-winter warming seen in calendar months reflects a later passage through freeze-up rather than a warmer lake within a given ice phase. LSWT falls rapidly during freeze-up, so a delay of the cooling curve by only a few days per decade produces sizeable trends at fixed calendar

https://doi.org/10.5194/egusphere-2026-6186
Preprint. Discussion started: 20 November 2026
© Author(s) 2026. CC BY 4.0 License.

dates. The optical ice record points to a delay of about this size, with freeze-up start and complete freeze-up shifting later by about 3 d per decade, although neither trend can be separated from interannual variability over 20 ice seasons (Table 2).

The coupling between LSWT and air temperature varied across ice stages (Fig. 5c). Under ice and during break-up, LSWT followed air temperature closely, as expected for an ice or snow surface, which stays much closer to the air temperature than open water does (Kirillin et al., 2012). During the open-water period, the heat capacity of the mixed layer dampened lake-surface responses, allowing deep lakes to buffer short-term atmospheric anomalies (Toffolon et al., 2014). Consequently, LSWT in the perennial water area changed little despite rising air temperatures. Coupling was weakest during freeze-up, when surface temperature was jointly regulated by heat release from the lake and transitions between ice-covered and open-water condition.

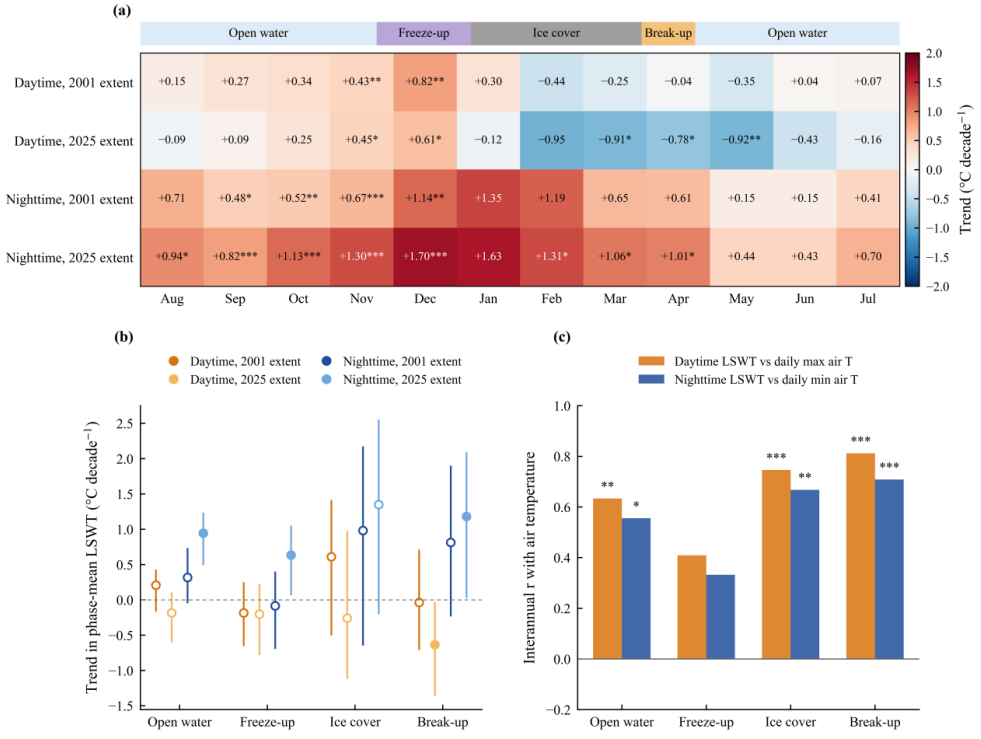



**Figure 5.** Seasonal and ice-regime structure of LSWT trends over Selin Co. (a) Monthly trends of daytime and nighttime LSWT within the 2001 and 2025 extents, arranged from August to July, with the typical timing of the ice phases shown above. (b) Trends of LSWT averaged over each ice phase, 2001–2020. (c) Interannual correlation between phase-mean LSWT and ERA5-Land air temperature (n = 20 ice seasons).

https://doi.org/10.5194/egusphere-2026-6186
Preprint. Discussion started: 20 November 2026
© Author(s) 2026. CC BY 4.0 License.

### 4.3 Coupling among air temperature, LSWT and lake ice

#### 4.3.1 Seasonal coupling between LSWT and air temperature

Throughout the annual cycle, LSWT remained higher than air temperature in every month and lagged air temperature by approximately three weeks (Fig. 6a, c). Under the same air temperature, lake water was several degrees warmer in autumn than in spring, producing a hysteresis loop (Fig. 6b). This pattern reflects seasonal heat storage: lake depth determines thermal inertia, causing surface cooling to lag behind atmospheric cooling (Toffolon et al., 2014; Leppäranta and Wen, 2022). After removing the seasonal cycle, the two series varied synchronously with no significant lag but showed only weak correlation, indicating that weather-scale air-temperature anomalies explained little of the day-to-day variation in LSWT (Fig. 6c).

The LSWT–air temperature difference reflects heat exchange during the freeze–thaw cycle (Fig. 6d–g). It peaked at approximately 12 °C three weeks before initial freeze-up. During freeze-up, the difference remained near 10 °C, as most of the lake was still open water and continued releasing heat to the progressively cooling atmosphere. Once the lake became fully ice-covered, the surface shifted from water to ice and the temperature difference declined rapidly, reaching about 6 °C on the day of complete freeze-up and 4 °C one month later. At the onset of break-up, the difference decreased again, likely because initial ice breakup coincided with short-term atmospheric warming. By the end of break-up, the difference reached its minimum for the entire ice season, indicating the strongest lake–atmosphere coupling. After ice-off, LSWT and air temperature warmed synchronously, maintaining a small temperature difference.

https://doi.org/10.5194/egusphere-2026-6186
Preprint. Discussion started: 20 November 2026
© Author(s) 2026. CC BY 4.0 License.

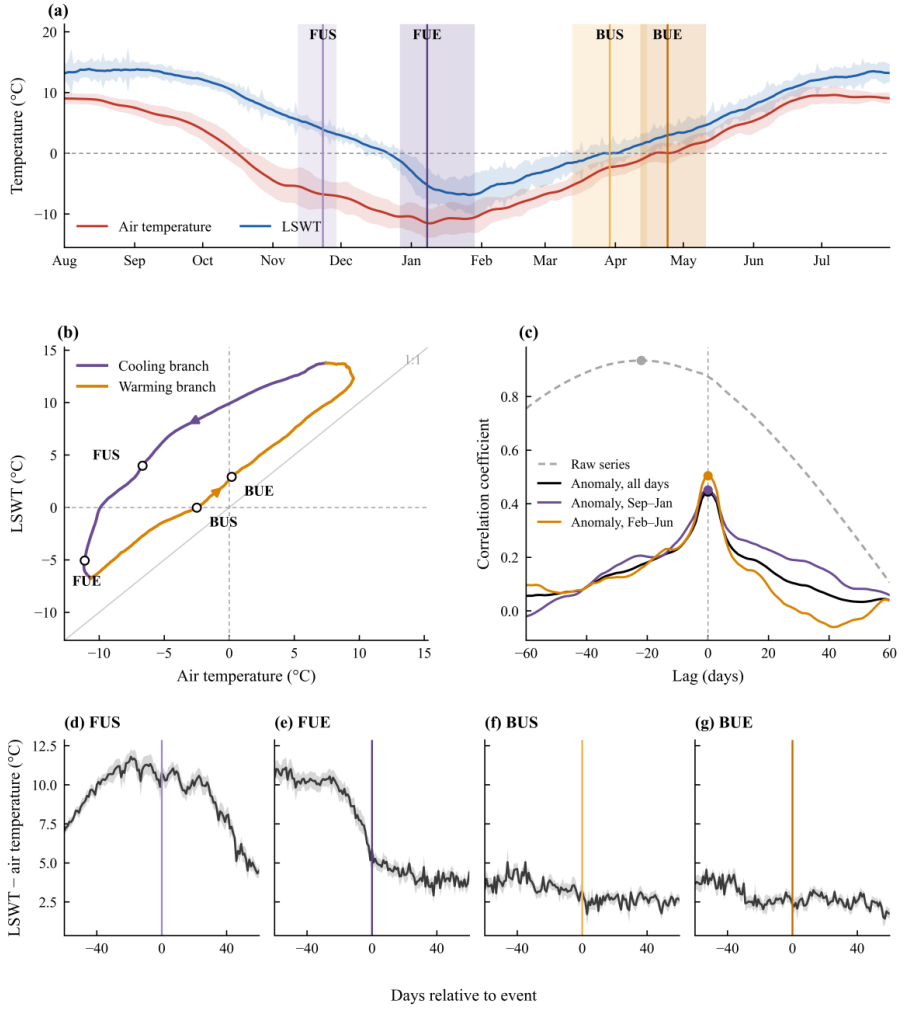



**Figure 6.** Seasonal coupling between LSWT and ERA5-Land air temperature,2001–2020. (a) Climatological annual cycle of LSWT and air temperature with the timing of the four ice events. (b) The same cycle plotted as LSWT against air temperature, separated into the cooling and warming branches, with the median dates of the ice events. (c) Cross-correlation of the raw series and of deseasonalized anomalies. (d–g) Difference between LSWT and air temperature from 60 d before to 60 d after each ice event, averaged over 20 ice seasons. FUS, freeze-up start; FUE, freeze-up end; BUS, break-up start; BUE, break-up end.

### 4.3.2 Ice regime and the freeze–thaw cascade

From 2001 to 2020, ice formation began in late November and reached complete freeze-up by early January, while break-up occurred from late March to late April (Fig. 6a). Freeze-up lasted ~46 days, nearly twice as long as break-up, with complete ice cover lasting ~81 days. Interannually, freeze-up onset (FUS) was the most stable, whereas break-up onset (BUS) varied

https://doi.org/10.5194/egusphere-2026-6186
Preprint. Discussion started: 20 November 2026
© Author(s) 2026. CC BY 4.0 License.

by over one month.

Tracking each ice season from the first sustained decline in air temperature below 0 °C shows that complete lake freeze-up is a ~12-week process rather than a direct response to cold-air onset (Fig. 7a, c). Ice first appeared about five weeks after air temperature turned below 0 °C, followed by LSWT reaching 0 °C roughly one month later and complete freeze-up another two weeks afterward. Ice typically formed first along shallow lake margins (Kropáček et al., 2013), while open water continued releasing heat. Break-up followed the reverse sequence (Fig. 7b, c): ice melt generally began ~3 weeks before sustained above-freezing air temperatures, approximately when LSWT returned to 0 °C, and complete ice-off occurred 21 d later.

LSWT and air temperature differed markedly at each ice event (Fig. 7d). At freeze-up onset, mean LSWT remained 4 °C while air temperature had fallen to −6 °C; complete freeze-up occurred during the coldest period, with air temperature below −10 °C. At break-up onset, LSWT was 1 °C while air temperature remained below freezing; complete ice-off occurred when air temperature approached 0 °C. Complete freeze-up corresponded to 580 °C·d cumulative freezing degree-days, relatively large and stable among years, whereas freeze-up onset occurred at 140 °C· d, with more than twice the relative variability. Both break-up events occurred before a marked increase in cumulative thawing degree-days.

Interannually, the timing of complete freeze-up was more closely related to the date when LSWT reached 0 °C than to when air temperature fell below 0 °C (Fig. 7e). Neither threshold crossing reliably predicted freeze-up onset, which itself varied little among years. Similarly, neither air- nor water-temperature threshold dates characterized the timing of either break-up event.

https://doi.org/10.5194/egusphere-2026-6186
Preprint. Discussion started: 20 November 2026
© Author(s) 2026. CC BY 4.0 License.

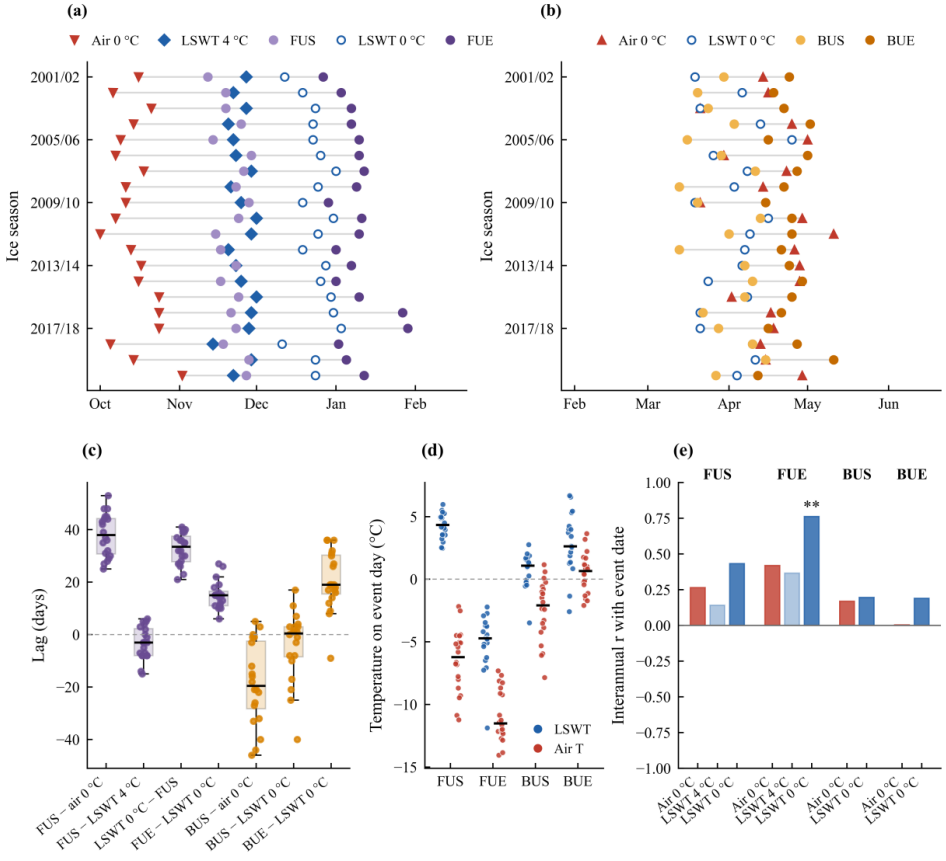



**Figure 7.** The freeze–thaw cascade of Selin Co, 2001–2020. (a, b) Sequence of the freeze-up and break-up cascades in each ice season. (c) Lags between successive steps of the cascade. (d) LSWT and air temperature on the day of each ice event. (e) Interannual correlation between each ice event and the dates on which air temperature and LSWT cross the indicated thresholds.

### 4.3.3 Water-column structure during freeze-up

In situ profiles from 2017 revealed the pre-freeze preparation of the lake (Fig. 8). In summer, the upper 15 m warmed to ~14 °C, while water at 38 m remained at 3–5.3 °C. From October, surface cooling deepened the mixed layer. When ice first formed on 23 November, the upper 28 m had become well mixed at ~5.4 °C, underlain by colder deep water. The water column was considered fully mixed when the temperature difference between 15 and 38 m was <0.3 °C; from 29 November onward, the entire water column was well mixed at 4.4 °C. Throughout the observation period, MODIS lake-wide mean LSWT closely tracked cooling in the upper water column (Fig. 8a).

Practical salinity derived from conductivity measurements was ~8. Using the Gibbs

https://doi.org/10.5194/egusphere-2026-6186
Preprint. Discussion started: 20 November 2026
© Author(s) 2026. CC BY 4.0 License.

Seawater Toolbox and the TEOS-10 equation of state (McDougall and Barker, 2011), places the temperature of maximum density of Selin Co water near 2.2 °C, in line with the empirical decrease of about 0.22 °C per unit of salinity (Kirillin et al., 2012), and its freezing point near −0.4 °C (Fig. 8c). Because salinity lowers the maximum-density temperature, the entire water column continued cooling below 4 °C, at about 0.09 °C $d^{-1}$ according to a linear regression, and reached 3.2 °C by mid-December without the inverse stratification that develops in fresh water once a lake cools past 4 °C (Fig. 8b). At this rate the open basin needed about 21 d to cool from 4 °C to its temperature of maximum density before a cold surface layer could form, consistent with complete freeze-up occurring only on 29 January 2018.

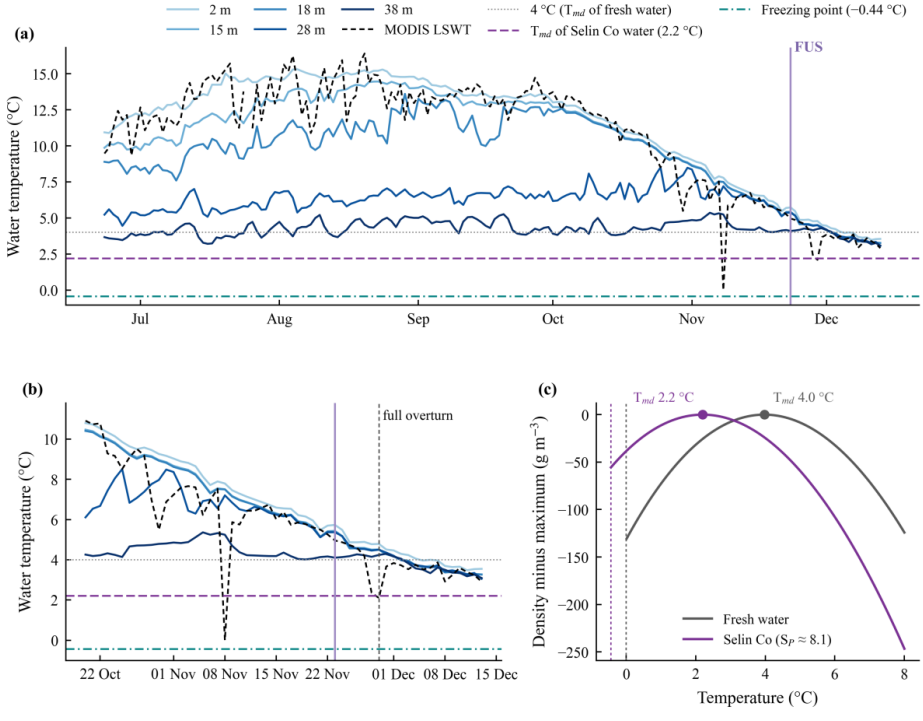



**Figure 8.** Water-column temperature of Selin Co during summer and autumn 2017 from loggers moored at 2–38 m depth. (a) Daily mean temperature at each depth and MODIS lake-mean LSWT (dashed), with the start of freeze-up of the 2017/18 ice season. (b) Detail of the autumn overturn and of the cooling below 4 °C. (c) Density of fresh water and of Selin Co water as a function of temperature.

### 4.3.4 LSWT thresholds as indicators of ice phenology

Dating ice events by an LSWT threshold of 0 °C placed freeze-up start about a month too late, complete freeze-up two weeks too early and break-up end three weeks too early, and only break-up start was dated without large bias (Fig. 9a). Event-specific threshold optimization

https://doi.org/10.5194/egusphere-2026-6186
Preprint. Discussion started: 20 November 2026
© Author(s) 2026. CC BY 4.0 License.

largely removed these biases (Fig. 9b; Table 2), but only optimized LSWT reproduced the observed interannual variability in complete freeze-up (Fig. 9c, d). Its optimal threshold was several degrees below 0 °C, reached only after most of the lake was ice-covered, because open water rarely cools far below its freezing point (Kirillin et al., 2012). For other events, optimized thresholds did not improve accuracy beyond climatological dates, and their derived trends differed from observations (Table 2).

**Table 2.** Performance of LSWT thresholds in dating the four ice events and trends of the event dates, 2001/02–2020/21 (n = 20 ice seasons). RMSE, r and p refer to the best threshold.

| Event | Best threshold (°C) | Bias at 0 °C (d) | RMSE (d) | Cross-validated RMSE (d) | r | p | SD of observed dates (d) | Trend of observed dates (d per decade) | Trend of LSWT-derived dates (d per decade) |
|---|---|---|---|---|---|---|---|---|---|
| FUS | 4.75 | 32.7 | 4.9 | 4.9 | 0.43 | 0.06 | 5 | +2.9 (0.33) | +2.8 (0.20) |
| FUE | −3.75 | −15.1 | 4.1 | 4.1 | 0.91 | < 0.001 | 8.2 | +3.4 (0.15) | +1.0 (0.60) |
| BUS | −0.50 | 4.1 | 12.1 | 14.4 | 0.39 | 0.09 | 10.4 | +6.6 (0.20) | +0.0 (0.97) |
| BUE | 2.75 | −20.6 | 10.3 | 13.2 | 0.23 | 0.32 | 6.7 | +0.0 (0.92) | +3.5 (0.49) |

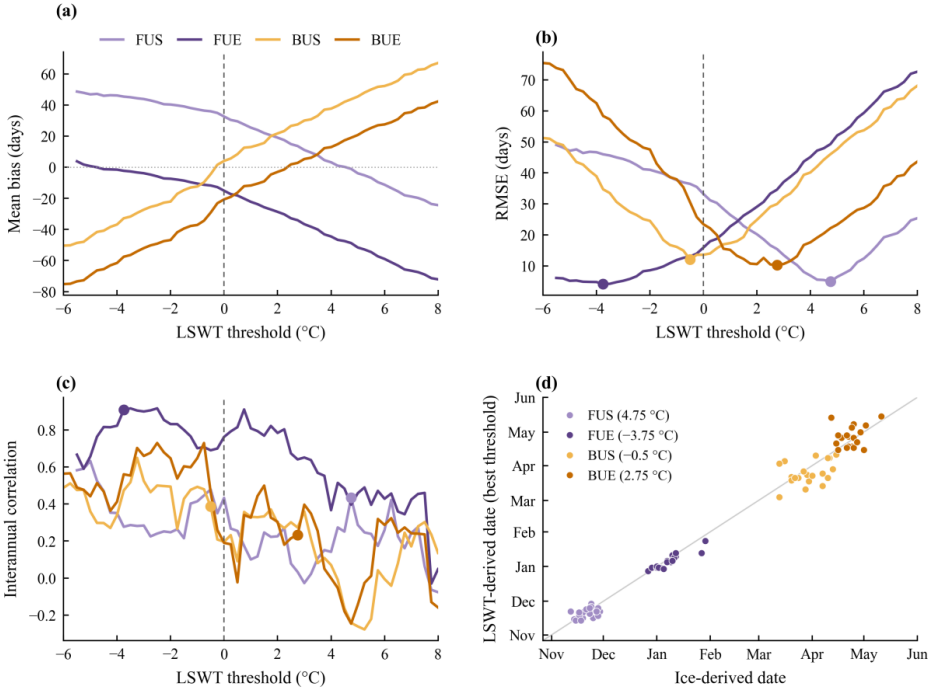



**Figure 9.** Performance of LSWT thresholds in dating the four ice events, 2001–2020. (a) Mean bias, (b) root-mean-square error and (c) interannual correlation between LSWT-derived and observed dates

https://doi.org/10.5194/egusphere-2026-6186
Preprint. Discussion started: 20 November 2026
© Author(s) 2026. CC BY 4.0 License.

as functions of the threshold. (d) LSWT-derived dates at the best threshold against observed dates.

#### 4.3.5 Controls on the interannual timing of ice events

To examine how ice-event timing relates to antecedent environmental conditions, we extracted air temperature, lake surface water temperature (LSWT), wind speed, shortwave radiation, and snowfall over 15-, 30-, and 60-day windows ending on the median event date, using means or cumulative values as appropriate. Additional cumulative windows were defined from 1 October for freeze-up events and from the median date of complete freeze-up (FUE) for break-up events. Fixed calendar windows were used to avoid defining predictors in relation to the events being explained. Pearson and partial correlations were calculated across 20 ice seasons. For partial correlations, air temperature was controlled for, except when air temperature itself was the predictor, in which case LSWT was controlled for. The Benjamini–Hochberg procedure (Benjamini and Hochberg, 1995) was applied to control the false discovery rate across 80 tests within each predictor category.

Complete freeze-up showed the strongest association with lake thermal state (Fig. 10). Higher LSWT during any antecedent window was associated with later complete freeze-up, with correlation coefficients of 0.81–0.88. The strongest correlations occurred over the preceding 1–2 months and remained nearly unchanged after controlling for air temperature. Air temperature was associated with complete freeze-up only over the 30-day window, and this relationship disappeared after controlling for LSWT. This suggests that atmospheric forcing does not directly control freeze-up, but acts through heat stored in the lake. After controlling for air temperature, stronger autumn winds were associated with earlier complete freeze-up. Freeze-up onset (FUS) showed no robust association with any tested variable, consistent with regression analyses of September LSWT.

Break-up timing was controlled mainly by cumulative winter and spring conditions rather than short-term conditions immediately before the events. Associations with environmental variables over the preceding 15–30 days were weak. Warmer winter and spring conditions, whether assessed over the preceding two months or the entire ice-covered period, were associated with earlier onset and completion of break-up. For break-up onset (BUS), air temperature, LSWT, and solar radiation covaried strongly; after controlling for air temperature, no variable retained an independent association at a 10% false discovery rate. Break-up completion (BUE) was most closely related to cumulative ice-surface temperature, and this relationship persisted after controlling for air temperature. Stronger solar radiation during the preceding two months was associated with earlier BUE, whereas snowfall tended to delay BUE.

https://doi.org/10.5194/egusphere-2026-6186
Preprint. Discussion started: 20 November 2026
© Author(s) 2026. CC BY 4.0 License.

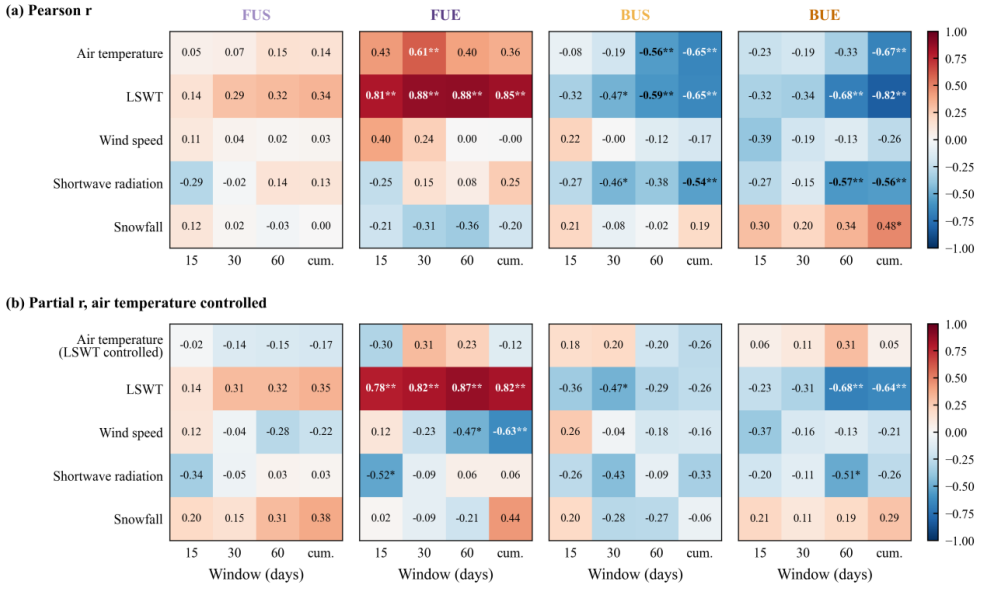



**Figure 10.** Correlation between the timing of each ice event and pre-event air temperature, LSWT, wind speed, shortwave radiation and snowfall over windows of different length. (a) Pearson correlation. (b) Partial correlation controlling for air temperature, or for LSWT in the air-temperature row. Cum., cumulative window starting on 1 October for freeze-up events and on the median FUE date for break-up events.

## 5 Discussion

### 5.1 Physical mechanisms for the breakdown of the 0 °C LSWT threshold over Selin Co

The 0 °C criterion fails at Selin Co for reasons rooted in the size, depth and salinity of the lake. Ice formed while lake-mean LSWT was still close to 4 °C. The lake covers ~2400 km² and reaches ~59 m in depth (Gyawali et al., 2019). Ice typically forms first along shallow bays and margins (Kropáček et al., 2013), where heat storage is limited, while the main open-water area continues releasing heat stored during summer for several weeks. At 1 km resolution, lake-wide LSWT is dominated by open water; thus, when optical imagery first detects ice, mean LSWT can remain well above the freezing point.

The salinity of the lake prolongs this phase. In fresh water, autumn convection stops when the lake has cooled to about 4 °C, the temperature of maximum density, because further cooling makes surface water lighter. A cold surface layer then forms and cools quickly to the freezing point while the deep water stays near 4 °C (Boehrer and Schultze, 2008; Kirillin et al., 2012). The salt content of Selin Co lowers the temperature of maximum density to about 2.2 °C, so convection continued through the range in which a freshwater lake would already be inversely

https://doi.org/10.5194/egusphere-2026-6186
Preprint. Discussion started: 20 November 2026
© Author(s) 2026. CC BY 4.0 License.

stratified, and the open basin had to lose the heat of roughly two further degrees of the entire water column before a freezable surface layer could form. At the cooling rate observed in December 2017, this step added about three weeks to the freeze-up of the open basin. The lowered freezing point of about −0.4 °C shifts the final step only slightly. By the time lake-mean LSWT reaches 0 °C, a large part of the lake has frozen, and complete freeze-up follows only after the surface has become ice and cooled several degrees further. In spring the situation reverses. An ice surface cannot warm above its melting point (Kirillin et al., 2012), so lake-mean LSWT returns to about 0 °C as soon as the surface begins to melt and open leads appear, which is why the start of break-up is the only event dated without large bias.

Therefore, a 0 °C LSWT threshold is unsuitable for Selin Co. Even after threshold calibration, only complete freeze-up retains meaningful interannual information, because only its surface temperature reliably indicates ice presence. Regional studies have applied the 0 °C threshold to MODIS land-surface temperature products (Shi et al., 2024), whereas others have calibrated lake-specific thresholds against optical ice maps for multiple Tibetan Plateau lakes (Wu et al., 2022). Threshold applicability likely depends on lake depth and salinity, which determine how long open water remains above its freezing point after ice first appears. In closed-basin lakes, salinity changes with water balance; thus, the expansion of Selin Co may itself alter its maximum-density temperature and freezing point. Salinity has declined as lake area expanded in the Selin Co basin (Zhu et al., 2019, 2025), consistent with similar hypotheses proposed for other saline Tibetan lakes whose ice phenology deviates from regional trends (Leppäranta and Wen, 2022; Cai et al., 2022.

### 5.2 The lake as a thermal mediator between atmosphere and ice

T The freeze-up sequence indicates that the atmosphere regulates lake-ice formation through the lake's thermal state. About 87 days elapsed between the first sustained sub-zero air temperatures and complete freeze-up. Complete freeze-up required roughly four times the freezing degree-days of ice onset, but showed less than half its relative variability. Its timing was closely related to the date when LSWT reached 0 °C; after controlling for LSWT, its association with antecedent air temperature disappeared, whereas its dependence on LSWT persisted after controlling for air temperature. This is characteristic of a heat-storage buffering system. Salinity further strengthens this buffering in Selin Co by allowing convection to continue cooling to ~2.2 °C rather than ~4 °C in freshwater. Ice-phenology models show that the lag between air-temperature cooling and freeze-up increases with lake depth and is also modulated by solar radiation (Leppäranta and Wen, 2022). Across the Tibetan Plateau, freeze-

https://doi.org/10.5194/egusphere-2026-6186
Preprint. Discussion started: 20 November 2026
© Author(s) 2026. CC BY 4.0 License.

up timing is likewise more strongly controlled by lake-specific physical properties than by regional climate conditions (Cai et al., 2019). Warm autumns delay freeze-up mainly by retaining more heat within the water column, while 15–60-day air-temperature anomalies act primarily by modifying the rate of heat loss. The annual hysteresis loop and the ~22-day phase lag of LSWT behind air temperature provide further evidence of this buffering effect (Schmid et al., 2014; Kirillin et al., 2017). Modeling studies of large Tibetan lakes similarly indicate that freeze-up timing depends on accumulated summer and autumn heat storage (Su et al., 2019; Wu et al., 2024).

The ice-phase decomposition of the LSWT trends points to the same mechanism. Calendar warming in November and December was large, yet the thermal state of the lake within the freeze-up phase did not change. During freeze-up lake-mean LSWT falls by about 0.2 °C $d^{-1}$, from about 4 °C at freeze-up start to about −5 °C at complete freeze-up. A delay of only 3 days per decade in the two freeze-up events (Table 2) can raise LSWT at fixed calendar dates by ~0.6 °C per decade, matching the November–December trend range (Fig. 5a). Thus, a simple shift of the autumn cooling trajectory can produce an apparent warming trend in calendar-month statistics, even without any change in the underlying seasonal trajectory. Only after controlling for air temperature did complete freeze-up show an association with cumulative wind speed, potentially reflecting wind-driven turbulent heat loss (Brown and Duguay, 2010), although longer observations or lake modeling are needed to confirm this mechanism.

### 5.3 Decoupling of ice break-up from air temperature

Break-up behaved differently from freeze-up. The first fracturing typically occurred about three weeks before air temperature turned persistently positive, before any appreciable thawing degree-days had accumulated, and neither break-up event followed the dates of the air or LSWT crossings. Their timing was related instead to the warmth of the preceding winter and spring and, for the end of break-up, to solar radiation independently of air temperature. Because snow cover on lake ice is generally sparse, strong winter radiation can penetrate the ice and warm the underlying water, allowing ice to thin from below even while air temperatures remain below freezing (Kirillin et al., 2021). In Tibetan lakes, melting begins while the air is still about 10 °C below the freezing point and the ice breaks up when air temperature has only just reached it, as observed here at the end of break-up, so degree-day approaches are biased where solar radiation dominates the heat balance (Leppäranta and Wen, 2022). Solar radiation has also been identified as the leading factor of lake-ice phenology in a MODIS study of lakes in Northeast China (Shi et al., 2024). Snowfall tended to delay complete ice-off, potentially because snow-

https://doi.org/10.5194/egusphere-2026-6186
Preprint. Discussion started: 20 November 2026
© Author(s) 2026. CC BY 4.0 License.



covered ice has higher albedo, although this relationship was weak. Previous studies of Tibetan Plateau lakes found that freeze-up is more strongly controlled by thermal conditions than break-up (Kropáček et al., 2013), consistent with our observations. The abrupt rise in air temperature on the day of break-up onset further suggests that warming events can trigger the final failure of an already weakened ice cover, while surface melting may cause optical remote sensing to identify this phenological transition earlier (Guo et al., 2018).

### 5.4 Uncertainties and limitations

LSWT during the ice season records the temperature of the ice or snow surface rather than the water, which explains why complete freeze-up and break-up end are related to it but also means that winter LSWT trends describe the ice surface. ERA5-Land air temperature over lake cells is partly shaped by the reanalysis lake scheme, which can hold near-surface air temperature up while the simulated lake is open and near 0 °C while simulated ice melts. Repeating the analyses with air temperature from a land ring 10–30 km outside the lake left the main conclusions unchanged. Complete freeze-up still followed the lake surface more closely than the air, its dependence on LSWT persisted after controlling for air temperature, and break-up still began weeks before the air warmed above 0 °C. The association of break-up end with solar radiation was also no longer independent of air temperature. Lake-cell air temperature in ERA5-Land thus carries part of the lake signal and shortens apparent lags, which should be borne in mind when the reanalysis is used to relate lake ice to air temperature. The analysis of ice-event timing rests on 20 ice seasons, so individual correlations carry wide uncertainty, and we have relied on associations that survive control of the false discovery rate and agree with physical expectation.

The in-situ profiles cover a single autumn at one mooring and end before complete freeze-up, so the cooling of the open basin below the temperature of maximum density and the formation of the surface layer under freezing conditions were not observed directly. Salinity, freezing point and temperature of maximum density were derived from conductivity with a seawater-based equation of state, and the true values for the ionic composition of Selin Co may differ slightly.

Long-term in situ observations across lake sectors and depths remain scarce on the plateau, which limits the calibration of satellite LSWT and the validation of ice phenology. Future work could combine multi-depth automated profiling of temperature and ice, higher-resolution or multi-sensor thermal data that resolve mixed ice–water pixels, and one- or three-dimensional lake–ice models that close the energy budget and quantify the relative roles of lake–atmosphere

https://doi.org/10.5194/egusphere-2026-6186
Preprint. Discussion started: 20 November 2026
© Author(s) 2026. CC BY 4.0 License.

exchange, mixing and ice–albedo feedbacks.

## 6 Conclusions

This study integrates MODIS LSWT, ERA5-Land meteorological data, optical lake-ice observations, and in situ temperature and conductivity profiles to investigate the coupling among air temperature, LSWT, and lake ice during the freeze–thaw cycle of a large saline lake on the Tibetan Plateau. Within the permanent water extent, nighttime LSWT warmed by about 0.55 °C per decade while daytime LSWT showed no detectable trend, and the resulting narrowing of the DTD arose at the lake surface rather than in the atmosphere. The apparent warming detected in early winter from calendar-month statistics was largely attributable to delayed freeze-up. Approximately 87 days elapsed between the onset of sustained atmospheric cooling and complete freeze-up, during which the lake continuously released stored heat. The timing of complete freeze-up was much more strongly related to the lake's thermal state than to the onset of atmospheric cooling. Salinity lowers the temperature of maximum water density in Selin Co to approximately 2.2 °C, allowing convective cooling to continue below 4 °C in autumn and thereby extending the cooling period before ice formation in the open-water area. Break-up was largely decoupled from air temperature and was primarily controlled by accumulated winter–spring heat and radiation. When a 0 °C LSWT threshold was used to identify the four ice-phenology events, the retrieved dates for three events showed biases of 15–33 days. Satellite-derived LSWT remains an effective indicator of the lake's thermal state, but LSWT-based identification of lake-ice phenology requires thresholds that account for lake depth and salinity and should be validated against direct lake-ice observations.

## Code and data availability

The MODIS land surface temperature products MOD11A1 and MOD11A2 (Wan et al., 2021a, b) are available from the NASA Land Processes Distributed Active Archive Center, ERA5-Land (Muñoz Sabater, 2019) from the Copernicus Climate Data Store, the Selin Co lake-ice phenology dataset from Li et al. (2023), and the in-situ water temperature and conductivity data from the National Tibetan Plateau / Third Pole Environment Data Center (Wang, 2019).

## Author contributions

BH designed the study, processed the data, performed the analyses and wrote the manuscript draft. DS supervised the work and acquired funding. DL, JW, RW and YL reviewed and edited the manuscript.

## Competing interests

https://doi.org/10.5194/egusphere-2026-6186
Preprint. Discussion started: 20 November 2026
© Author(s) 2026. CC BY 4.0 License.

The contact author has declared that none of the authors has any competing interests.

**Acknowledgements**

We thank the National Tibetan Plateau / Third Pole Environment Data Center for providing the in situ water temperature and conductivity data of Selin Co.

**Financial support**

This research has been supported by the Key R&D Project of the Science and Technology Department of Tibet (grant no. XZ202501ZY0030), the Key Laboratory of Cryospheric Science and Frozen Soil Engineering (grant nos. CSFSE-ZZ-2402 and CSFSE-FX-250), the Shule River Basin Water Resources Utilization Center, Gansu Province (grant no. SLH/KYXM-2025-01), the National Natural Science Foundation of China (grant no. 42001068) and the Gansu Provincial Natural Science Foundation (grant no. 25JRRA502).

**References**

Benjamini, Y. and Hochberg, Y.: Controlling the false discovery rate: a practical and powerful approach to multiple testing, J. R. Stat. Soc. Ser. B Methodol., 57, 289–300, https://doi.org/10.1111/j.2517-6161.1995.tb02031.x, 1995.

Bibi, S., Wang, L., Li, X. P., Zhou, J., Chen, D. L., and Yao, T. D.: Climatic and associated cryospheric, biospheric, and hydrological changes on the Tibetan Plateau: a review, Int. J. Climatol., 38, E1–E17, https://doi.org/10.1002/joc.5411, 2018.

Boehrer, B. and Schultze, M.: Stratification of lakes, Rev. Geophys., 46, RG2005, https://doi.org/10.1029/2006RG000210, 2008.

Brown, L. C. and Duguay, C. R.: The response and role of ice cover in lake-climate interactions, Prog. Phys. Geogr., 34, 671–704, https://doi.org/10.1177/0309133310375653, 2010.

Cai, Y., Ke, C. Q., Li, X. G., Zhang, G. Q., Duan, Z., and Lee, H.: Variations of Lake Ice Phenology on the Tibetan Plateau From 2001 to 2017 Based on MODIS Data, J. Geophys. Res. Atmos., 124, 825–843, https://doi.org/10.1029/2018jd028993, 2019.

Cai, Y., Ke, C. Q., Xiao, Y., and Wu, J.: What caused the spatial heterogeneity of lake ice phenology changes on the Tibetan Plateau?, Sci. Total Environ., 836, 155517, https://doi.org/10.1016/j.scitotenv.2022.155517, 2022.

Chen, W., Yao, T., Zhang, G., Li, S., and Zheng, G.: Accelerated glacier mass loss in the largest river and lake source regions of the Tibetan Plateau and its links with local water

https://doi.org/10.5194/egusphere-2026-6186
Preprint. Discussion started: 20 November 2026
© Author(s) 2026. CC BY 4.0 License.



balance over 1976–2017, J. Glaciol., 67, 577–591, https://doi.org/10.1017/jog.2021.9, 2021.

Guo, L. N., Wu, Y. H., Zheng, H. X., Zhang, B., Li, J. S., Zhang, F. F., and Shen, Q.: Uncertainty and Variation of Remotely Sensed Lake Ice Phenology across the Tibetan Plateau, Remote Sens., 10, 1534, https://doi.org/10.3390/rs10101534, 2018.

Guo, L. N., Zheng, H. X., Wu, Y. H., Fan, L. X., Wen, M. X., Li, J. S., Zhang, F. F., Zhu, L. P., and Zhang, B.: An integrated dataset of daily lake surface water temperature over the Tibetan Plateau, Earth Syst. Sci. Data, 14, 3411–3422, https://doi.org/10.5194/essd-14-3411-2022, 2022.

Guo, L. N., Sun, W. B., Wu, Y. H., Xiong, J. F., and Jiang, J. N.: Investigation of Thermal Effects of Lakes on Their Adjacent Lands Across Tibetan Plateau Using Satellite Observation During 2000 to 2022, Remote Sens., 17, 3314, https://doi.org/10.3390/rs17193314, 2025.

Gyawali, A. R., Wang, J. B., Ma, Q. F., Wang, Y., Xu, T., Guo, Y., and Zhu, L. P.: Paleo-environmental change since the Late Glacial inferred from lacustrine sediment in Selin Co, central Tibet, Palaeogeogr. Palaeoclimatol. Palaeoecol., 516, 101–112, https://doi.org/10.1016/j.palaeo.2018.11.033, 2019.

Hou, G., Yuan, X., Wu, S., Ma, X., Zhang, Z., Cao, X., Xie, C., Ling, Q., Long, W., and Luo, G.: Phenological changes and driving forces of lake ice in Central Asia from 2002 to 2020, Remote Sens., 14, 4992, https://doi.org/10.3390/rs14194992, 2022.

Kirillin, G., Leppäranta, M., Terzhevik, A., Granin, N., Bernhardt, J., Engelhardt, C., Efremova, T., Golosov, S., Palshin, N., Sherstyankin, P., Zdorovennova, G., and Zdorovennov, R.: Physics of seasonally ice-covered lakes: a review, Aquat. Sci., 74, 659–682, https://doi.org/10.1007/s00027-012-0279-y, 2012.

Kirillin, G., Wen, L. J., and Shatwell, T.: Seasonal thermal regime and climatic trends in lakes of the Tibetan highlands, Hydrol. Earth Syst. Sci., 21, 1895–1909, https://doi.org/10.5194/hess-21-1895-2017, 2017.

Kirillin, G. B., Shatwell, T., and Wen, L.: Ice-covered lakes of Tibetan Plateau as solar heat collectors, Geophys. Res. Lett., 48, e2021GL093429, https://doi.org/10.1029/2021GL093429, 2021.

Kropáček, J., Maussion, F., Chen, F., Hoerz, S., and Hochschild, V.: Analysis of ice phenology of lakes on the Tibetan Plateau from MODIS data, The Cryosphere, 7, 287–

https://doi.org/10.5194/egusphere-2026-6186
Preprint. Discussion started: 20 November 2026
© Author(s) 2026. CC BY 4.0 License.



301, https://doi.org/10.5194/tc-7-287-2013, 2013.

Kuang, X. X. and Jiao, J. J.: Review on climate change on the Tibetan Plateau during the last half century, J. Geophys. Res. Atmos., 121, 3979–4007, https://doi.org/10.1002/2015jd024728, 2016.

Lei, Y. B., Zhou, J., Yao, T. D., Bird, B. W., Yu, Y. F., Wang, S. J., Yang, K., Zhang, Y. S., Zhai, J. Q., and Dai, Y. F.: Overflow of Siling Co on the central Tibetan Plateau and its environmental impacts, Sci. Bull., 69, 2829–2832, https://doi.org/10.1016/j.scib.2024.07.035, 2024.

Leppäranta, M. and Wen, L.: Ice phenology in Eurasian lakes over spatial location and altitude, Water, 14, 1037, https://doi.org/10.3390/w14071037, 2022.

Li, X. Y., Peng, S. S., Xi, Y., Woolway, R. I., and Liu, G.: Earlier ice loss accelerates lake warming in the Northern Hemisphere, Nat. Commun., 13, 5156, https://doi.org/10.1038/s41467-022-32830-y, 2022.

Li, J., Cao, Z., Hu, M., Xiong, J., and Ma, R.: A dataset of lake ice distribution in Lake Selin Co on the Tibet Plateau from 2000 to 2021, China Sci. Data, 8, https://doi.org/10.11922/11-6035.csd.2023.0099.zh, 2023 (in Chinese).

McDougall, T. J. and Barker, P. M.: Getting started with TEOS-10 and the Gibbs Seawater (GSW) Oceanographic Toolbox, SCOR/IAPSO WG127, ISBN 978-0-646-55621-5, 2011.

Moreira, S., Schultze, M., Rahn, K., and Boehrer, B.: A practical approach to lake water density from electrical conductivity and temperature, Hydrol. Earth Syst. Sci., 20, 2975–2986, https://doi.org/10.5194/hess-20-2975-2016, 2016.

Murfitt, J. and Brown, L. C.: Lake ice and temperature trends for Ontario and Manitoba: 2001 to 2014, Hydrol. Process., 31, 3596–3609, https://doi.org/10.1002/hyp.11295, 2017.

Muñoz-Sabater, J., Dutra, E., Agustí-Panareda, A., Albergel, C., Arduini, G., Balsamo, G., Boussetta, S., Choulga, M., Harrigan, S., Hersbach, H., Martens, B., Miralles, D. G., Piles, M., Rodríguez-Fernández, N. J., Zsoter, E., Buontempo, C., and Thépaut, J. N.: ERA5-Land: a state-of-the-art global reanalysis dataset for land applications, Earth Syst. Sci. Data, 13, 4349–4383, https://doi.org/10.5194/essd-13-4349-2021, 2021.

Nonaka, T., Matsunaga, T., and Hoyano, A.: Estimating ice breakup dates on Eurasian lakes using water temperature trends and threshold surface temperatures derived from MODIS data, Int. J. Remote Sens., 28, 2163–2179, https://doi.org/10.1080/01431160500391957,

https://doi.org/10.5194/egusphere-2026-6186
Preprint. Discussion started: 20 November 2026
© Author(s) 2026. CC BY 4.0 License.



2007.

Piccolroaz, S., Zhu, S., Ladwig, R., Carrea, L., Oliver, S., Piotrowski, A. P., Ptak, M., Shinohara, R., Sojka, M., Woolway, R. I., and Zhu, D. Z.: Lake Water Temperature Modeling in an Era of Climate Change: Data Sources, Models, and Future Prospects, Rev. Geophys., 62, e2023RG000816, https://doi.org/10.1029/2023RG000816, 2024.

Qiu, Y. L., Chen, J., Chen, D. L., Thiery, W., Mercado-Bettín, D., Xiong, L. H., Xia, J., and Woolway, R. I.: Enhanced heating effect of lakes under global warming, Nat. Commun., 16, 3954, https://doi.org/10.1038/s41467-025-59291-3, 2025.

Rouse, W. R., Oswald, C. M., Binyamin, J., Blanken, P. D., Schertzer, W. M., and Spence, C.: Interannual and seasonal variability of the surface energy balance and temperature of central Great Slave Lake, J. Hydrometeorol., 4, 720–730, https://doi.org/10.1175/1525-7541(2003)004<0720:IASVOT>2.0.CO;2, 2003.

Schmid, M., Hunziker, S., and Wüest, A.: Lake surface temperatures in a changing climate: a global sensitivity analysis, Clim. Change, 124, 301–315, https://doi.org/10.1007/s10584-014-1087-2, 2014.

Shi, X., Cheng, J., Yang, Q., Li, H., Hao, X., and Wang, C.: Variations of lake ice phenology derived from MODIS LST products and the influencing factors in Northeast China, Remote Sens., 16, 4025, https://doi.org/10.3390/rs16214025, 2024.

Shi, X. D., Wang, B. B., Ma, Y. M., Sun, L. J., Li, W. M., Lazhu, Hu, Z. Y., Zuo, H. C., Li, X., and Chen, M. S.: A Comprehensive Study on the Ice Freeze-Thaw Process in a High-Elevation Large Lake of the Tibetan Plateau, J. Geophys. Res. Atmos., 130, e2024JD042750, https://doi.org/10.1029/2024JD042750, 2025.

Su, D. S., Hu, X. Q., Wen, L. J., Lyu, S. H., Gao, X. Q., Zhao, L., Li, Z. G., Du, J., and Kirillin, G.: Numerical study on the response of the largest lake in China to climate change, Hydrol. Earth Syst. Sci., 23, 2093–2109, https://doi.org/10.5194/hess-23-2093-2019, 2019.

Toffolon, M., Piccolroaz, S., Majone, B., Soja, A. M., Peeters, F., Schmid, M., and Wüest, A.: Prediction of surface temperature in lakes with different morphology using air temperature, Limnol. Oceanogr., 59, 2185–2202, https://doi.org/10.4319/lo.2014.59.6.2185, 2014.

Tong, Y., Feng, L., Wang, X. C., Pi, X. H., Xu, W., and Woolway, R. I.: Global lakes are warming slower than surface air temperature due to accelerated evaporation, Nat. Water,

https://doi.org/10.5194/egusphere-2026-6186
Preprint. Discussion started: 20 November 2026
© Author(s) 2026. CC BY 4.0 License.



1, 929–940, https://doi.org/10.1038/s44221-023-00148-8, 2023.

Wan, Z.: New refinements and validation of the collection-6 MODIS land-surface temperature/emissivity product, Remote Sens. Environ., 140, 36–45, https://doi.org/10.1016/j.rse.2013.08.027, 2014.

Wan, W., Zhao, L., Xie, H., Liu, B., Li, H., Cui, Y., Ma, Y., and Hong, Y.: Lake Surface Water Temperature Change Over the Tibetan Plateau From 2001 to 2015: A Sensitive Indicator of the Warming Climate, Geophys. Res. Lett., 45, 11177–11186, https://doi.org/10.1029/2018gl078601, 2018.

Wang, J.: Temperature and conductivity data of Selincuo Lake (2017), National Tibetan Plateau / Third Pole Environment Data Center [data set], https://doi.org/10.11888/Hydro.tpdc.270083, 2019.

Wang, X., Shi, K., Qin, B., Zhang, Y., and Woolway, R. I.: Disproportionate impact of atmospheric heat events on lake surface water temperature increases, Nat. Clim. Change, 14, 1172–1177, https://doi.org/10.1038/s41558-024-02122-y, 2024.

Woolway, R. I., Kraemer, B. M., Lenters, J. D., Merchant, C. J., O'Reilly, C. M., and Sharma, S.: Global lake responses to climate change, Nat. Rev. Earth Environ., 1, 388–403, https://doi.org/10.1038/s43017-020-0067-5, 2020.

Woolway, R. I., Jennings, E., Shatwell, T., Golub, M., Pierson, D. C., and Maberly, S. C.: Lake heatwaves under climate change, Nature, 589, 402–407, https://doi.org/10.1038/s41586-020-03119-1, 2021.

Wu, Y., Guo, L., Zhang, B., Zheng, H., Fan, L., Chi, H., Li, J., and Wang, S.: Ice phenology dataset reconstructed from remote sensing and modelling for lakes over the Tibetan Plateau, Sci. Data, 9, 743, https://doi.org/10.1038/s41597-022-01863-9, 2022.

Wu, Y., Huang, A. N., Li, X., Wen, L. J., Lazhu, and Li, J. Y.: Thermal Response of Large Seasonally Ice-Covered Lakes Over Tibetan Plateau to Climate Change, J. Geophys. Res. Atmos., 129, e2023JD039935, https://doi.org/10.1029/2023JD039935, 2024.

Xu, H. Q.: Modification of normalised difference water index (NDWI) to enhance open water features in remotely sensed imagery, Int. J. Remote Sens., 27, 3025–3033, https://doi.org/10.1080/01431160600589179, 2006.

Xu, F. L., Zhang, G. Q., Woolway, R. I., Yang, K., Wada, Y., Wang, J. D., and Crétaux, J. F.: Widespread societal and ecological impacts from projected Tibetan Plateau lake expansion, Nat. Geosci., 17, 516–523, https://doi.org/10.1038/s41561-024-01446-w,

https://doi.org/10.5194/egusphere-2026-6186
Preprint. Discussion started: 20 November 2026
© Author(s) 2026. CC BY 4.0 License.

2024.

Yao, T. D., Bolch, T., Chen, D. L., Gao, J., Immerzeel, W., Piao, S., Su, F. G., Thompson, L., Wada, Y., Wang, L., Wang, T., Wu, G. J., Xu, B. Q., Yang, W., Zhang, G. Q., and Zhao, P.: The imbalance of the Asian water tower, Nat. Rev. Earth Environ., 3, 618–632, https://doi.org/10.1038/s43017-022-00299-4, 2022.

Yao, F. F., Livneh, B., Rajagopalan, B., Wang, J. D., Crétaux, J. F., Wada, Y., and Berge-Nguyen, M.: Satellites reveal widespread decline in global lake water storage, Science, 380, 743–749, https://doi.org/10.1126/science.abo2812, 2023.

Zhang, K. X. and Yao, Y. L.: Lake Heatwaves and Cold-Spells Across Qinghai-Tibet Plateau Under Climate Change, J. Geophys. Res. Atmos., 128, e2023JD039243, https://doi.org/10.1029/2023JD039243, 2023.

Zhang, X., Wang, K., and Kirillin, G.: An automatic method to detect lake ice phenology using MODIS daily temperature imagery, Remote Sens., 13, 2711, https://doi.org/10.3390/rs13142711, 2021.

Zhang, G., Wang, M., Zhou, T., and Chen, W.: Progress in remote sensing monitoring of lake area, water level, and volume changes on the Tibetan Plateau, Natl. Remote Sens. Bull., 26, 115–125, https://doi.org/10.11834/jrs.20221171, 2022 (in Chinese).

Zhou, J., Wang, L., Zhang, Y. S., Guo, Y. H., Li, X. P., and Liu, W. B.: Exploring the water storage changes in the largest lake (Selin Co) over the Tibetan Plateau during 2003–2012 from a basin-wide hydrological modeling, Water Resour. Res., 51, 8060–8086, https://doi.org/10.1002/2014wr015846, 2015.

Zhu, L. and Wang, J.: A Comprehensive Scientific Survey Report on Environmental Changes in the Serling Co Region, Tibet, Science Press, Beijing, 2021 (in Chinese).

Zhu, L. P., Ju, J. T., Qiao, B. J., Liu, C., Wang, J. B., Yang, R. M., Ma, Q. F., Guo, L. N., and Pang, S. Y.: Physical and biogeochemical responses of Tibetan Plateau lakes to climate change, Nat. Rev. Earth Environ., 6, 284–298, https://doi.org/10.1038/s43017-025-00650-5, 2025.